Quantitative video microscopy of patch clamped membranes stress, strain, capacitance, and stretch channel activation

Masahiro Sokabe, Frederick Sachs, and Zhongqi Jing
Department of Biophysical Sciences, State University of New York at Buffalo, Buffalo, New York 14214 USA

ABSTRACT Membrane patches from chick skeletal muscle were stretched by applying controlled suction or pressure to the pipette. From images of the patch, the patch dimensions (area and radius of curvature) were computed by nonlinear regression of the images to a geometric model. With no applied pressure, patch membranes are nearly planar and normal to the wall of the pipette. With increasing pressure gradients, the patch bulges, the radius of curvature decreases, and the area increases. The patch capacitance changes in exact proportion to the change in area at a rate of 0.7 $\mu F/cm^2$. The increase in area is due to a flow of lipid (with perhaps small amounts of diffusible protein) along the walls of the pipette into the patch. The flow is reversible with a relaxation of the pressure gradient. The area elastic constant of the membrane is ~50 dyn/cm, insensitive to cytochalasin B and probably represents the elasticity of the underlying spectrin/dystrophin network. Simultaneous measurements of stretch activated (SA) ion channel activity in the patch showed that the sensitivity of channels from different patches, although different when calculated as a function of applied pressure, was the same when calculated as a function of tension. Because patch lipid is free to flow, and hence stress-free in the steady state, SA channels must be activated by tension in the cytoskeleton.

INTRODUCTION

Since the first description of stretch activated (SA) channels in cultured chick muscle cells (1), they have been reported in almost every organism and tissue including *E. coli*, yeast, higher plants, invertebrates, vertebrates (2–6), oocytes, epithelia, endothelial cells, skeletal muscle cells, smooth muscle cells, and neurones (7–12).

Although there is good reason to believe that SA channels are activated by membrane tension (13), there has never been a direct measurement of the tension. Instead, channel activity is usually measured as a function of the pressure applied to the patch pipette and a proportionality is assumed between pressure and tension. We report here the simultaneous measurement of patch geometry, capacitance, and channel activation which permit the calculation of membrane stress, strain, and its influence on SA channel activation. The results confirm that SA channels are activated by membrane tension, not transmural pressure. Tension is coupled to the channel through an elastic cytoskeleton, perhaps spectrin, not through tension in the lipid bilayer. Furthermore, the data shows that the radius of the patch varies with applied pressure and that lipids are free to flow along the walls of the pipette into the patch.

To obtain clear images of the patch, we used high magnification, differential interference contrast microscopy with additional video magnification. The pipettes were made from thin wall borosilicate glass, and the tips were bent to be nearly parallel to the stage (14). We made patches only from the side of cells to reduce interference arising from the underlying image of the cell itself. To manipulate the pipette, we used three orthogonal motorized slides (Newport Electronics, Inc., Santa Ana, CA) driven by a low vibration controller (15). To reduce thermal drift and movement of the pipette due to changes in pressure, we clamped it rigidly to a quartz rod mounted on the manipulator. The pipette holder floated between the patch amplifier and the back of the pipette. Pipette pressure was applied with an oil filled servo which had a rise time of a few milliseconds.

We chose cultured chick muscle cells as a source of SA channels because their properties have been well documented (1). Under gentle suction (0.5–1 cm Hg; 1 cm Hg = 1.33 kPa), a bleb of cell was drawn into the pipette forming a gigaseal when the patch was 5–25 μm from the tip. We employed medium size pipettes (tip diameter, 0.8–1 μm; resistance, 4–6 MΩ) and studied patches located 8–15 μm from the tip (cf. Fig. 1). From these, we selected for analysis only those patches which were axially symmetric, as judged by through-focus images.

Typical patch images obtained with different pres-

Masahiro Sokabe's present address is Department of Physiology, Nagoya University School of Medicine, Nagoya 466, Japan

0006-3495/91/03/722/07 $2.00

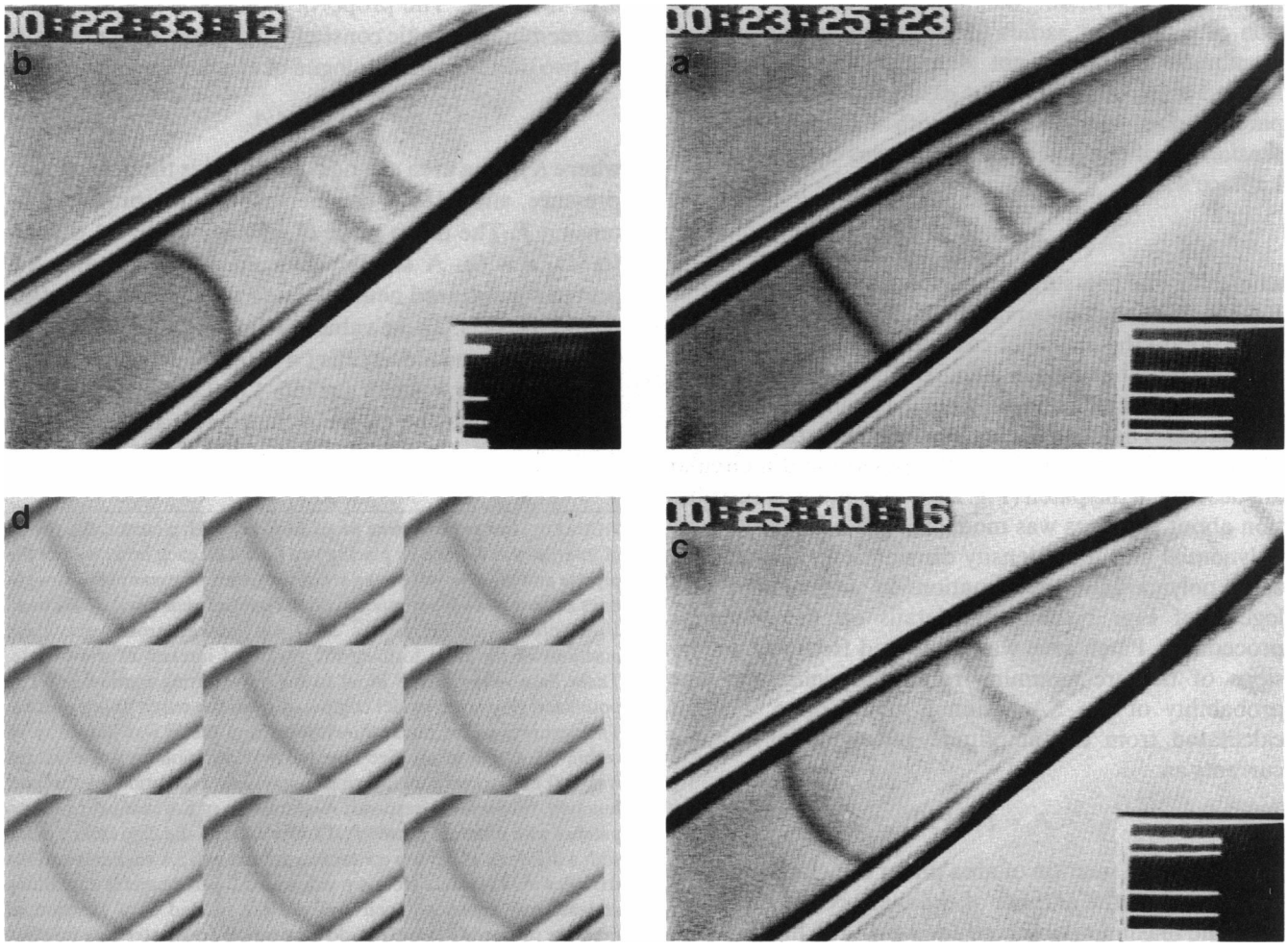

FIGURE 1 Typical patch images with different pressures. (*a*) 0 cm Hg; (*b*) +1.0 cm Hg; (*c*) −1.0 cm Hg. The reference of 0 cm Hg was set by adjusting the pressure until flow of solution through the pipette was zero (judged by the movement of debris in the recording chamber). Note the large change in the radius of patch curvature with pressure. (*d*) A time series (500 ms/frame, *left to right, top to bottom*) showing the shape change after a pressure pulse (−1.44 cm Hg 5 s duration) which started at the second frame. Notice the large amount of cytoplasm present in the pipette as well as vesicular structures. This is typical of patches viewed with both light and electron microscopy (14, 34). Images were stored on S-VHS tape, digitized with a computer controlled frame grabber (DT 2851) and printed with a thermal video printer (Mitsubishi, Tokyo, Japan). The final magnification in the frame buffer was ~30 nm/pixel. The video time code and analogue data (pressure, patch current, capacity, voltage, etc.) are superimposed on the upper left and lower right in the screen, respectively. Synchronization between the image and the analogue data was made by relaying the video time code via a homemade hardware converter, through the computer's serial port to the comment field of the acquisition software (PCLAMP; Axon Instruments, Inc., Burlingame, CA). Methods: We modified a standard inverted microscope (model IMT-II; Olympus, Lake Success, NY) with a 100× oil immersion objective (NA 1.4) to use a 50× water immersion objective (E. Leitz, Inc., Rockleigh, NY) (NA 1.0, working distance [WD] 0.68 mm) as the condenser. The halogen illuminator was replaced by the Olympus mercury burner. The parforcalizing TV-coupling lens (×0.3) was removed to increase magnification. The image of the patch was projected on a model CCD camera with a 6.3× photo eyepiece (Cohu Inc., San Diego, CA). Cultured chick skeletal muscle cells were prepared according to standard methods (1) and were usually used after 1–2 weeks in culture. 10 min before the experiment, the culture medium was replaced with normal saline (150 NaCl; 5 KCl; 2 $CaCl_2$; 1 $MgCl_2$; 10 Hepes, pH 7.4). Pipettes were filled with the same solution. Experiments were done at room temperature (20–25°C) in cell-attached configuration. Pipettes were pulled from 1.4 mm thin wall borosillicate glass (100λ Microcaps; Drummond Scientific Co., Broomall, PA) using a programmable micropipette puller (model PC-84; Sutter, San Raphael, CA) with a seven step program.

sures are shown in Fig. 1, *a–c*. One striking feature of these images is that the radius of curvature is pressure dependent. This finding contradicts the common assumption of a constant radius of curvature and shows that membrane tension is not simply proportional to the applied pressure (1). In most cases, the curvature of the patch surface was well fitted with a circular arc. The tension, T, of the patch membrane was calculated from Laplace's law,

$$T = PR/2, \quad (1)$$

where P is the pressure difference across the patch, and R is the radius of the curvature of the patch.

To obtain the radius of curvature and the patch area we digitized the image and, then used a nonlinear regression routine to fit the data to a geometric model of the patch. The model consisted of two straight lines describing the inner walls of the pipette and a circular arc describing the patch (Fig. 2 *a*). The intensity distribution about the lines was modeled with a biphasic cubic polynomial and the intensity distribution about the arc as a polynomial approximation to a Gaussian (see legend of Fig. 2 for more details on the modeling procedure). Patch area was computed from the dimensions of the arc assuming rotational symmetry. The probability of the SA channels being open, P_o, was calculated from the amplitude histogram of channel currents as,

$$P_o = 1 - P_c^{(1/N)}, \quad (2)$$

where P_c is the fraction of area under the closed channel peak, and N is the number of channels. N was estimated from the maximum observed level with the highest level of stimulation and may be underestimated.

RESULTS

Fig. 2 *e* shows the dose-response curves for SA channels from two patches with different diameters. The solid symbols and the associated solid lines (linear least-squares regression) represent activity as a function of membrane tension. The open symbols and associated dashed lines (linear regression), represent the activity as a function of applied pressure. The sensitivity of channels from different patches is nearly the same when the independent variable is tension, but not when the independent variable is pressure. This result suggests that much of the variability found between different patches may represent uncertainty in the actual stimulus.

The mechanical properties of the patch were studied by examining the relationship between the membrane tension, the membrane area, and the membrane capacitance. When the membrane tension increases the patch area increases. The proportionality between the two is the membrane elastic constant. This was calculated from the two dimensional analogue of Hooke's law (16),

$$T = K_a \Delta A/A, \quad (3)$$

where K_a is the area elastic constant, A is the area at zero pressure, and ΔDA is the increase in area produced by tension T. The mean value of K_a was 48.3 ± 6.1 dyn/cm (±SD, $n = 6$). A similar value has been recently reported for cultured neurons using the pipette aspiration technique (17). These values are much lower than those observed for red blood cells ($\approx$250–500 dyn/cm) (18, 19) or lipid bilayer vesicles ($\approx$150–1,000 dyn/cm) (20, 21). We believe that the elasticity represents the properties

FIGURE 2 Image processing procedure. (*a*) With a cursor, the region of interest was defined by placing two points on each inner wall of the pipette and three points on the arc of the patch. The computed straight lines and arc were superimposed on the image (*white lines*). (*b*) A band 10–15 pixels wide (12 in this case) was marked around the mean positions of the lines forming the region of interest as shown in *c*. These data were used as input to the curve fitting routine. (*d*) The optimized geometric model computed from the curve fitting routine. The accuracy of the linear dimensions from the fit was judged to be within 5% of the mean (See note below). Precision on single images was ~0.1%, corresponding single precision evaluation of the cost function. (*e*) Stimulus-response relationships of SA channel from two patches with different geometry. Circles indicate the data from a patch with a diameter of 4.5 μm containing at least two SA channels and the triangles indicate data from a patch with 5.2 μm diameter containing at least one channel. Open symbols are plotted as a function of pressure squared (P^2) and the closed symbols are plotted as a function of tension (T^2). Each line was determined by linear regression. Note that as a function of tension, the sensitivity of the two patches is nearly identical (10.82 and 10.77 (dyn/cm)^2/e-fold change in P_o). As a function of applied pressure, the sensitivities vary (3.55 and 2.55 cm^2 Hg/e-fold change in P_o). The elastic constant (K_a) of the two patches was similar (~50 dyn/cm). Note: calibration of geometric parameters. To trust the absolute value of the patch capacitance it was necessary to verify the absolute dimensions derived from the fitting procedure. We calibrated the video system in x and y using a stage micrometer. Errors due to the cylindrical lens effect of the pipette were checked using a ray tracing program (BEAM-3; Stellar Software, Berkeley, CA) to model the effect of geometrical distortion. This proved to be <3%, worst case. To locate where the pipette walls were physically located relative to the intensity distribution of the inner wall (see Fig. 1), we deposited calibrated latex beads (3–7 μm in diameter; Polysciences, Inc., Warrington, PA) in the pipettes and measured their diameter with a modified version of the fitting program which just fit the intensity distribution of the pipette walls. When the fitted lines were extrapolated to the middle of the bead, the distance between them estimated the bead diameter. The result of this analysis using several groups of different sized beads was that the physical diameter of the pipette was a few percent wider than the distance between the intensity minima located over the inner walls. The patch dimensions were scaled accordingly.

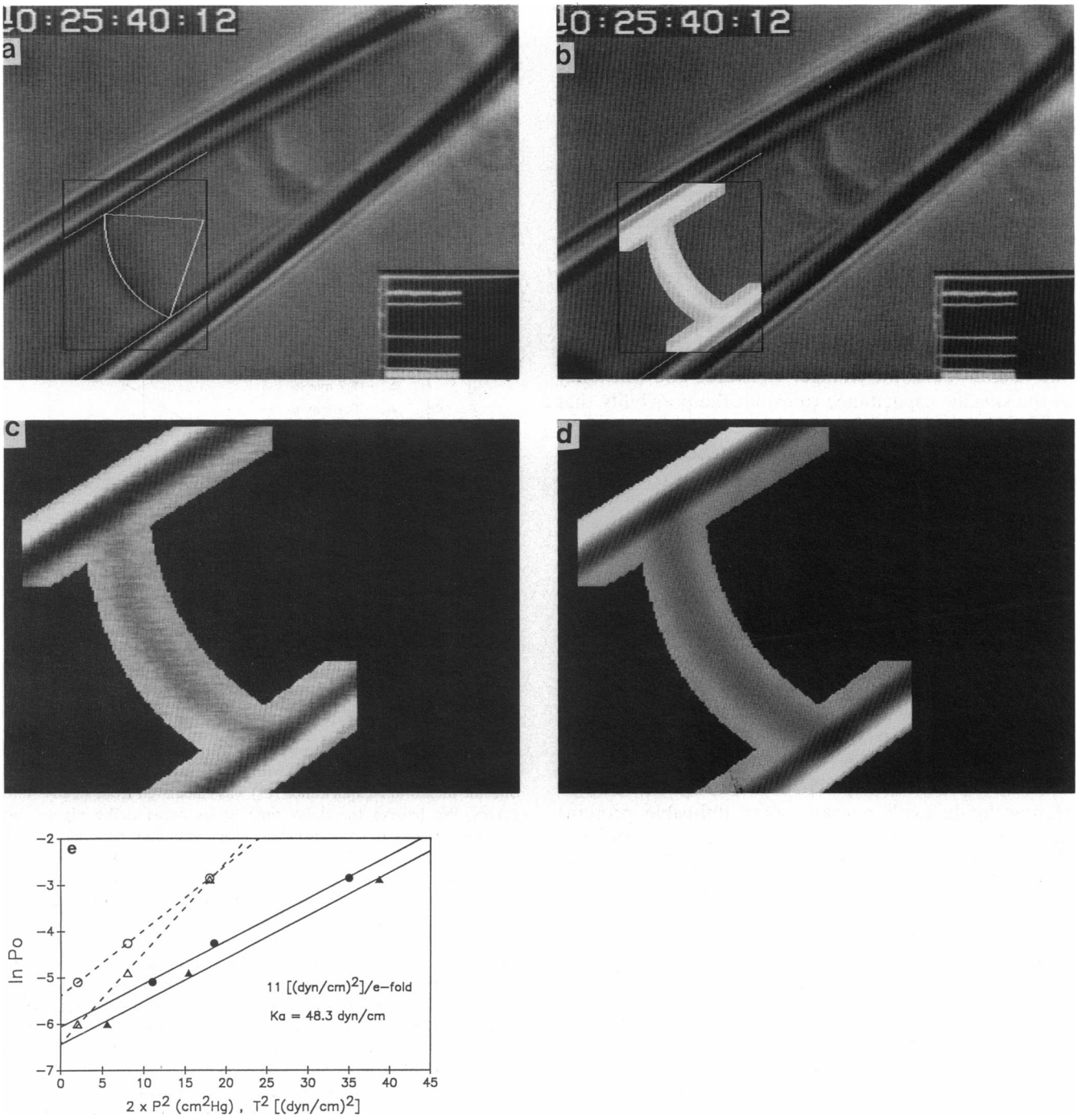

of the membrane linked cytoskeleton. Pretreatment of the cells (overnight) with 10^{-5}M cytochalasin B did not significantly affect the value of K_a (47 ± 7.4 dyn/cm, n = 9), suggesting that the elastic elements are not actin based. The elasticity may be that of the submembrane spectrin network known to exist in these cells (22).

The increase in patch area with pressure could arise from three sources: unfolding of unresolved membrane pleats, stretching of a fixed amount of membrane, or the influx of new membrane. We tested these alternatives by measuring the capacitance during changes in area. Capacitance was measured at 10 kHz using a phaselock amplifier (23). The results are shown in Fig. 3 *a*. The patch capacitance increased after an increase in pressure. As previously reported (24), the capacitance increased sigmoidally with a delay time of a few hundred milliseconds followed by an exponential rise to a steady-state value (Fig. 3). The time constant of the rising phase

was ~1 s. The falling phase was first order and had a time constant of ~800 ms. The increase in capacitance observed with applied pressure rules out the possibility that the increase in area comes from the unfolding of unresolved pleats.

From sequentially acquired patch images after a step of pressure (Fig. 1 *d*), we measured the change in area associated with the change in capacitance (Fig. 3 *a*, *top trace*). Like the capacitance, the area increased with a time constant of 1 s after a short latency (Fig. 3 *a*, *dashed line*). Plotting the change in capacitance against the change in area yields a straight line with a slope of 0.7 $\mu F/cm^2$ (Fig. 3 *b*). There is an essentially perfect correlation between area and capacitance irrespective of time and magnitude of the change. The value and constancy of the specific capacitance rules out the possibility that the increase in area comes from stretching the lipids. If the membrane lipids were being stretched, the specific capacitance would have increased with area (the specific capacitance of a constant volume membrane increases linearly with the area). Additionally, the increase in patch area (>10%) is far in excess of the strain that leads to lysis of lipid membranes (2–3%) (25–27). The specific capacitance of 0.7 $\mu F/cm^2$ is lower than the 1–1.2 $\mu F/cm^2$ often cited for protein containing biological membranes (28). Phospholipid/cholesterol membranes, however, have a specific capacitance of ≈ 0.6 $\mu F/cm^2$ (29) and the addition of a small amount of protein with a higher dielectric constant (10?) would raise the specific capacitance to 0.7 $\mu F/cm^2$.

Thus, the increase in patch area comes from an influx of new lipids (with perhaps some diffusible protein) from stores along the walls of the pipette, and in the case of cell-attached patches, from the cell itself (30). (Excised patches behave similarly to cell-attached patches.) Electron microscopic images of patch pipettes (31) show a sheet of membrane lying along the wall. Because the patch area does not increase indefinitely, but exhibits a characteristic elastic constant, there must be cytoskeletal (or possibly extracellular) structures spanning the patch. These are visible in electron microscope images of patches (31–34). The elasticity of these structures provides the energy to retract the patch when tension is reduced.

DISCUSSION

The data shown here provide strong support for the coupling of SA channels to the cytoskeleton. Because there is little strain in the membrane lipid, then the SA channels must be attached to some other tension bearing element. Because neither tubulin or actin reagents block SA channel activation (1), we suspect that the

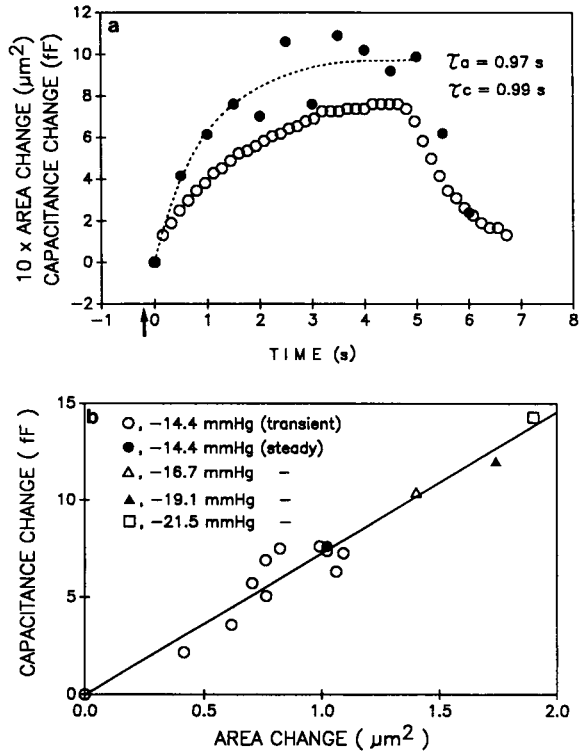

FIGURE 3 (*a*) Simultaneous recording of the time course of the change in area (*solid circles*) and capacitance (*open circles*) of a patch membrane in response to a negative pressure pulse (−1.44 cm Hg, 5 s duration) applied at −0.2 s (*arrow*). After 200 ms delay, both the area and capacitance start to increase after a single exponential (indicated by dashed line for area change) with similar time constants (τ_a and τ_c). Specific membrane capacitance (C_s) was calculated from steady-state values. We believe the delay time arises because the pipette tip contains viscoelastic cytoplasm which prevents fluid flow into the tip for short times, i.e., the intracellular face of the patch is not at atmospheric pressure for several hundred milliseconds after applying pressure to the pipette. The time course of the change in capacitance/area is probably dominated by viscous drag between membrane lipids and immobilized membrane proteins and possibly between the lipids and the walls of the pipette. (*b*) Correlation between capacitance change and area change. The data indicated with open circles were taken from *a* (transient response) and other data were taken from steady-state values at with different amounts of pressure. Correlation coefficient (*r*) was 0.97 and the specific patch capacitance calculated from the slope was 0.75 $\mu F/cm^2$. Methods. Patch currents were measured with an Axon Instruments, Inc. Axopatch 1-C amplifier. Changes in patch capacitance were measured using a phaselock amplifier at 10 kHz. The phase was set by adjusting the fast capacity compensation and time constant to completely cancel the carrier signal. The system was then unbalanced using the fast capacity compensation and the amplifier locked to the phase of the resulting signal. The output time constant was set to 30 ms. The capacitance was scaled to 1 fF/200 mV with a 20 mV rms carrier. We found that the gain of the Axon Instruments Inc. 1-B and 1-C patch clamps depends upon the input load at 10 kHz, and that the error is not fully corrected by transient compensation. We calibrated the load dependence and found that with a transient compensated 10 pF load, the true capacity was 119% of the uncorrected value, (Sigurdson, W. J., M. Sokabe and F. Sachs, manuscript in preparation).

spectrin/dystrophin submembrane cytoskeleton is the tension bearing element.

The data also provide some information on the nature of the gigaseal. The casual flow of lipids from the patch to the walls of the pipette eliminate models of seal formation that involve strong coupling of lipids to the glass (35). Because the seal region in our experiments did not move and the lipids did, we must assume that the attachment to the glass involves membrane proteins. It is not hard to imagine membrane proteins denaturing against the high energy surface of the glass and thereby anchoring the membrane structure to the pipette. The lipid can then flow around these anchoring proteins like a river flowing around bridge piers. The high resistance of the seal can be accounted for if the space between the membrane and the glass is filled, like a sucrose gap, with the sugar residues of surface glycoproteins (36). Because liposomes can make seals to pipettes, we must conclude that either the seal is a dynamic process that allows sliding or the mechanism is made by a different mechanism. For example, in tip-dip pipettes and giant liposomes, the path length between the membrane and the glass may be hundreds of microns (Sokabe, M., unpublished data).

The data in this paper have lead us to reinterpret some results of earlier experiments. Sachs (24) proposed that the increase in patch capacitance with stress was due to lipid strain. That interpretation is clearly not correct. Another striking disagreement with earlier data is the lack of cytochalasin effects on elasticity. Guharay and Sachs (1) showed a large increase in SA channel sensitivity with cytochalasin treatment. We are not sure of the origin of the discrepancy, but we think that it arises from the way cytoplasmic viscosity affects patch formation. Implicit in the earlier analysis is the assumption that the radius of curvature of the patch was the same in the presence and absence of cytochalasins. The earlier experiments employed steeply tapered pipettes, whereas the experiments reported here used narrow, slowly tapering, pipettes. Because cytochalasin softens the cytoplasm, we suspect that with the steeply tapering pipettes, the soft cytoplasm leads to larger diameter patches with larger radii of curvature and hence greater sensitivity. With slowly tapering pipettes, the change in diameter with aspiration distance is small. Unfortunately, we were not able to image the steeply tapered pipettes with the current system to verify this idea.

The change in radius of curvature with pressure has implications for the functional relationship between P_o and applied pressure. Some papers have reported that P_o is an exponential function of pressure and others that P_o is an exponential function of pressure squared (13). Because the radius of curvature decreases with pressure, low pressures will produce more activity per increment in pressure than will high pressures, thereby lowering the slope of the dose-response relationship. More recent modeling indicates that both linear and quadratic terms should be present (39). Although the data on P_o in this paper are plotted to emphasize a squared dependence on tension (Fig. 2), the data is insufficient to comprise a test of the functional form. More extensive measurements are in progress.

We would like to thank R. Borschel for innumerable pieces of machine work, D. Borkowski for design and construction of the time code reader and its relevant software and the pressure clamp, and H. Zhou for work on the original software for fitting images. Portions of this work have appeared in abstract form (37, 38).

Supported by National Institute of Diabetes and Digestive and Kidney Diseases DK-37792, the Muscular Dystrophy Association, The United States Army Research Office, 22560-LS, and Japanese ministry of education (01880028, 01570044).

Received for publication 29 June 1990 and in final form 5 November 1990.

REFERENCES

1. Guharay, F., and F. Sachs. 1984. Stretch-activated single ion channel currents in tissue-cultured embryonic chick skeletal muscle. *J. Physiol. (Lond.).* 352:685–701.
2. Martinac, B., M. Buechner, A. H. Delcour, J. Adler, and C. Kung. 1987. Pressure-sensitive ion channel in *Escherichia coli. Proc. Natl. Acad. Sci. USA.* 84:1–5.
3. Gustin, M. C., B. Martinac, Y. Saimi, M. R. Culbertson, and C. Kung. 1986. Ion channels in yeast. *Science (Wash. DC).* 233:1195–1197.
4. Edwards, K. L., and B. G. Pickard. 1987. Detection and transduction of physical stimulii in plants. *In* The cell surface in signal transduction. E. Wagner, H. Greppin, and B. Millet, editors. Springer-Verlag, Berlin. 41–66.
5. Sigurdson, W. J., C. E. Morris, B. L. Brezden, and D. R. Gardner. 1987. Stretch activation of aK+ channel in molluscan heart cells. *J. Exp. Biol.* 127:191–209.
6. Stockbridge, L. L., and A. S. French. 1988. Stretch-activated cation channels in human fibroblasts. *Biophys. J.* 54:187–190.
7. Methfessel, C., V. Witzemann, T. Takahashi, M. Mishina, S. Numa, and B. Sakmann. 1986. Patch clamp measurements on Xenopus laevis oocytes: currents through endogenous channels and implanted acetylcholine receptor and sodium channels. *Pfluegers Arch. Eur. J. Physiol.* 407:577–588.
8. Cooper, K. E., J. M. Tang, J. L. Rae, and R. S. Eisenberg. 1986. A cation channel in frog lens epithelia responsive to pressure and calcium. *J. Membr. Biol.* 93:259–269.
9. Lansman, J. B., T. Hallam, and T. J. Rink. 1987. Single stretch-activated ion channels in vascular endothelial cells as mechanotransducers. *Nature (Wash. DC).* 325:811–813.
10. Brehm, P., R. Kullberg, and F. Moody-Corbett. 1984. Properties of non-junctional acetylcholine receptor channels on innervated muscle of Xenopus Laevis. *J. Physiol. (Lond.).* 350:631–648.
11. Kirber, M. T., J. V. Walsh, and J. J. Singer. 1988. Stretch-activated

ion channels in smooth muscle: a mechanism for the initiation of stretch-induced contraction. *Pfluegers Arch. Eur. J. Physiol.* 12:339–345.

12. Morris, C. E., and W. J. Sigurdson. 1989. Stretch-inactivated ion channels coexist with stretch-activated ion channels. *Science (Wash. DC).* 243:807–809.
13. Sachs, F. 1988. Mechanical transduction in biological systems. *Crit. Rev. Biomed. Eng.* 16:141–169.
14. Sokabe, M., and F. Sachs. 1990. The structure and dynamics of patch-clamped membranes: a study by differential interference microscopy. *J. Cell Biol.* 111:599–606.
15. Gao, X., and F. Sachs. 1989. Improving performance of motorized slides for micromanipulation. *J. Neurosci. Methods.* 28:225–227.
16. Helfrich, W. 1973. Elastic properties of lipid bilayers: theory and possible experiments. *Z. Naturforsch. Teil. C Biochem. Biophys. Biol. Virol.* 28C:693–703.
17. Horie, H., and S. Ikuta. 1989. Neuronal cell membranes become rigid with age. *Biophysics (Japan).* 29:191–194.
18. Evans, E., R. Waugh, and L. Melnik. 1976. Elastic area compressibility modulus of red cell membrane. *Biophys. J.* 16:585.
19. Evans, E. A., R. Waugh, and L. Melnik. 1976. Elastic area compressibility modulus of red cell membrane. *Biophys. J.* 16:585–594.
20. Evans, E., and D. Needham. 1986. Giant vesicle bilayers composed of mixtures of lipids, cholesterol and polypeptides. *Faraday Discuss. Chem. Soc.* 81:267–280.
21. Evans, E., and D. Needham. 1987. Physical properties of surfactant bilayer membranes: thermal transitions, elasticity, rigidity, cohesion, and colloidal interactions. *J. Phys. Chem.* 91:4219–4228.
22. Repasky, E. A., C. M. Pollina, M. M. Menold, and M. S. Hudecki. 1986. Increased concentration of spectrin is observed in avian dystrophic muscle. *Proc. Natl. Acad. Sci. USA.* 83:802–806.
23. Neher, E., and A. Marty. 1982. Discrete changes of cell membrane capacitance observed under conditions of enhanced secretion in bovine adrenal chromaffin cells. *Proc. Natl. Acad. Sci. USA.* 79:6712–6716.
24. Sachs, F. 1987. Baroreceptor mechanisms at the cellular level. *Fed. Proc.* 46:12–16.
25. Kwok, R., and E. Evans. 1981. Thermoelasticity of large lecithin bilayer vesicles. *Biophys. J.* 35:637–652.
26. Wolfe, J., and P. Steponkus. 1981. The stress-strain relation of the plasma membrane of isolated plant protoplasts. *Biochim. Biophys. Acta.* 643:662–668.
27. Wolfe, J., M. Dowgert, and P. Steponkus. 1986. Mechanical study of the deformation and rupture of the plasma membranes of protoplasts during osmotic expansions. *Membr. Biol.* 93:63–74.
28. Cole, K. S. 1972. Membranes ions and impulses. University of California Press, Berkeley, CA. 569 pp.
29. Macintosh, T., S. A. Simon, and J. Dilger. 1989. Location of the water-hydrocarbon interface in lipid bilayers. *In:* From model membranes to isolated cells. G. Benghe, editor. CRC Press, Boca Raton, FL. 1–13.
30. Milton, R. L., and J. H. Caldwell. 1990. Na current in membrane blebs: implications for channel mobility and patch clamp recording. *J. Neurosci.* 10:885–893.
31. Sachs, F., and M. Song. 1987. High-voltage electron microscopy of patch-clamped membranes. *Proc. Electron Microsc. Soc. Am.* 45:582–583.
32. Jung, F., M. J. Song, and F. Sachs. 1987. Patch clamp anatomy: high voltage electron microscopy of in vivo patches. *Biophys. J.* 51:517a. (Abstr.)
33. Ruknudin, A., M. Song, A. Auerbach, and F. Sachs. 1989. The structure of patch clamped membranes in high voltage electron microscopy. *Proc. Electron Microsc. Soc. Am.* 47:936–937.
34. Ruknudin, A., M. J. Song, and F. Sachs. 1990. The ultrastructure of patch clamped membranes: a study using high voltage electron microscopy. *J. Cell. Biol.* In press.
35. Corey, D. P., and C. F. Stevens. 1983. Science and technology of patch recording electrodes. *In* Single Channel Recording. B. Sakmann, and E. Neher, editors. Plenum Publishing Corp. New York. 53–68.
36. Sachs, F. 1984. The noise produced by patch electrodes: a model. *Biophys. J.* 45:57a. (Abstr.)
37. Sachs, F., and M. Sokabe. 1989. Stress and strain in patch clamped membranes. *Int. Conf. Video Microsc.* 37a. (Abstr.)
38. Sokabe, M., and F. Sachs. 1988. Imaging patches and simultaneous recording of stretch activated channel activity. *Int. Congr. Comp. Physiol. Biochem.* 815.
39. Sachs, F., and H. Lecar, 1991. Models for mechanical transduction. *Biophys. J.* In press.